JOURNAL OF SOLID STATE CHEMISTRY **122,** 111–117 (1996)
ARTICLE NO. 0090

On the $Na_xNi_{0.6}Co_{0.4}O_2$ System: Physical and Electrochemical Studies

I. Saadoune,* A. Maazaz,* M. Ménétrier,† and C. Delmas†,[1]

*Université Cadi-Ayyad, Laboratoire de Chimie du Solide Minéral, Faculté des Sciences-Semlalia, B. P. S15, Marrakesh, Morocco; and †Institut de Chimie de la Matière Condensée de Bordeaux and Ecole Nationale Supérieure de Chimie et Physique de Bordeaux, Avenue Dr. A. Schweitzer, 33608 Pessac Cedex, France

Received August 7, 1995; accepted October 31, 1995

Sodium chemical deintercalation from the $NaNi_{0.6}Co_{0.4}O_2$ phase was realized by using iodine as oxidizing agent. The $Na_{0.58}Ni_{0.6}Co_{0.4}O_2$ phase obtained was used as the positive electrode in sodium batteries. Several structural transformations were observed during discharge (intercalation reaction). The magnetic and electrical study of the $Na_xNi_{0.6}Co_{0.4}O_2$ ($x = 1$, 0.80, 0.58) phases shows clearly that Ni^{III} ($t_{2g}^6e^1$ in LS configuration) is preferentially oxidized to the tetravalent state compared to Co^{III} ($t_{2g}^6e^0$ in LS configuration). The sodium diffusion coefficient was also calculated in the solid solution domains. It shows that the diffusion kinetics is faster when sodium ions are situated in a prismatic environment.

INTRODUCTION

Although most of the efforts in the development of nonaqueous electrolyte secondary batteries have pointed toward lithium insertion materials (1–3), a large variety of layered $NaMX_2$ materials (M = transition metal and X = O, S) (4–7) exhibit interesting fundamental properties, very different from those of the homologous lithiated phases. Even if the MX_2 slabs are almost identical, the strong differences in size and electronegativity of Li and Na induce very different electrochemical behavior. $NaNiO_2$ (8) and $LiNiO_2$ (9) layered oxides give a typical example of this divergence.

On the other hand, several studies have shown that sodium can be deintercalated chemically and electrochemically from layered $NaMO_2$ compounds at room temperature (10), leading to the formation of some Na_xMO_2 bronzes which are difficult to obtain at high temperature.

Previous surveys have investigated the $NaNi_{1-y}Co_yO_2$ system (11). It has been demonstrated that the existence of this solid solution is limited to $y = 0.5$ even though $NaNi_{0.5}Co_{0.5}O_2$ and $NaCoO_2$ phases have relatively comparable cell parameters. These lamellar oxides have been used as precursor materials to obtain oxyhydroxides which are active materials in Ni ‖ Cd secondary batteries (11).

As previously reported, the $NaNi_{1-y}Co_yO_2$ ($0 \leq y \leq 0.2$) phases exhibit a monoclinic symmetry similar to that of $NaNiO_2$ (8), whereas, in the $0.2 \leq y \leq 0.5$ composition range, the materials crystallize in the α-$NaFeO_2$-type structure with a rhombohedral unit cell. The $LiNi_{1-y}Co_yO_2$ homologous phases exhibit a rhombohedral symmetry throughout the whole composition range. In order to compare the physicochemical properties of both $ANi_{1-y}Co_yO_2$ (A = Na, Li) systems, we have selected the $NaNi_{0.6}Co_{0.4}O_2$ phase, which has a symmetry identical to that of the $LiNi_{1-y}Co_yO_2$ system, for this study. This paper presents the results obtained by the electrochemical and physical studies of the $NaNi_{0.6}Co_{0.4}O_2$ phase. Furthermore, we will discuss the relationship between the sodium diffusion kinetics and the nature of the oxygen packing.

EXPERIMENTAL

The $NaNi_{0.6}Co_{0.4}O_2$ oxide was synthesized as described in Ref. (11) from an intimately ground mixture of Na_2O, Co_3O_4, and NiO, heated in pure dry oxygen for 10 h at 600°C, then for 48 h at 800°C. Because of a loss of sodium oxide due to evaporation during the reaction, a 5% excess of this oxide was added in order to obtain the desired stoichiometry.

Sodium deintercalation was performed chemically and electrochemically. For the chemical deintercalation, $NaNi_{0.6}Co_{0.4}O_2$ was oxidized using iodine in acetonitrile solution. The oxidized product was washed with acetonitrile and methanol, under pure argon, to remove sodium halides and was dried under vacuum.

For the electrochemical study, an $Na/NaClO_4$ (1 M) in a propylene carbonate/$Na_xNi_{0.6}Co_{0.4}O_2$ cell was used. A small quantity of Ketjenblack was added to the positive electrode material in order to increase the macroscopic electronic conductivity.

X-ray diffraction data on the $Na_xNi_{0.6}Co_{0.4}O_2$ phases

[1] To whom correspondence should be addressed.

0022-4596/96 $18.00

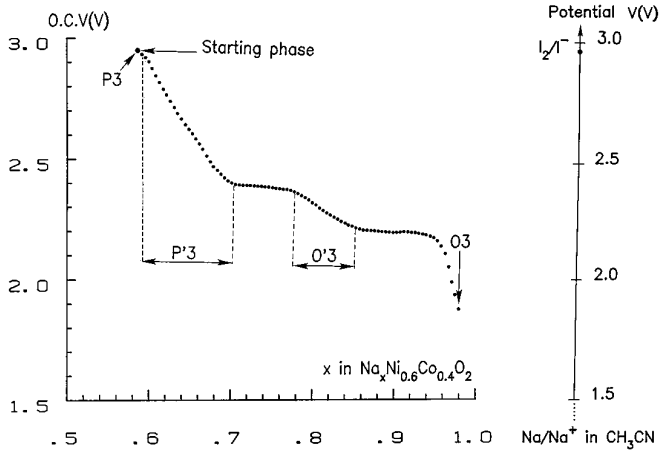

FIG. 1. Open circuit voltage vs composition of the Na‖$Na_xNi_{0.6}Co_{0.4}O_2$ cell.

were collected on an "INEL curve position-sensitive detector" using cobalt $K\alpha$ radiation. It should be noted that all these experiments were performed in sealed capillaries (under dry argon), since the $Na_xNi_{0.6}Co_{0.4}O_2$ phases are very hygroscopic.

The magnetic susceptibility measurements were carried out using a DSM 5 (Manics) susceptometer. A four-probe method was used for the electrical conductivity measurements.

RESULTS AND DISCUSSION

Electrochemical Behavior

The X-ray pattern of the nominal $NaNi_{0.6}Co_{0.4}O_2$ phase was indexed in the trigonal space group $R\bar{3}m$ with hexagonal parameters: $a_{hex.} = 2.950(1)$ Å and $c_{hex.} = 15.84(1)$ Å. This oxide, like isomorphous AMO_2 layered oxides (A = Li, Na and M = Cr, Co, Ni) (10), exhibits an ordered rocksalt structure in which the sodium and M cations reside in alternate layers of a cubic close-packed oxide anion array (O3-type structure) (12).

After chemical oxidation of this phase, a black product with the composition $Na_{0.58}Ni_{0.6}Co_{0.4}O_2$ was obtained. With the aim of minimizing the electrolyte degradation phenomenon, which is generally observed in sodium batteries during charge (9), the chemically deintercalated sample, $Na_{0.58}Ni_{0.6}Co_{0.4}O_2$, was used as starting phase in the Na‖$Na_xNi_{0.6}Co_{0.4}O_2$ cell instead of the $NaNi_{0.6}Co_{0.4}O_2$ oxide.

Figure 1 shows the evolution of the open circuit voltage vs composition x during the cell discharge. The thermodynamic potential of the starting phase is 2.94 V, which corresponds approximately to the potential of the I/I^- redox couple vs that of Na^+/Na (13). This shows the potentiostatic character of the chemical intercalation/deintercalation reactions. In contrast to the lithium homologous phases (14), several structural transformations were observed during discharge. As shown in Fig. 1, two potential plateaus, at 2.4 and 2.1 V, which correspond to two-phase domains, were also observed. These evolutions in the OCV composition curve are similar to those evidenced in the Na_xCoO_{2-y} system (15). In the latter system, the composition scale differs from one Na‖Na_xCoO_{2-y} electrochemical cell to another, depending on the y value. Yet, for all materials, the plateaus are obtained at the same voltages. The maximum amount of intercalation (at discharge) corresponds, for each y value, to the $O3$-type phase in which the oxidation state of cobalt ions is nearly +III. In the case of mixed nickel cobalt materials, no evidence of an oxygen nonstoichiometry has ever been reported.

X-Ray Characterization

The X-ray study has been focused on four materials: the starting phase $Na_{0.58}Ni_{0.6}Co_{0.4}O_2$, the compositions corresponding to the center of each solid solution domain (x = 0.65, x = 0.80), and the final $Na_{0.98}Ni_{0.6}Co_{0.4}O_2$ phase. The last composition corresponds to the most intercalated phase obtained by electrochemical intercalation. The sequence of the X-ray diffraction patterns of $Na_xNi_{0.6}Co_{0.4}O_2$ (x = 0.98, x = 0.80, x = 0.65, x = 0.58) phases is given in Fig. 2. The two extreme phases, $Na_{0.98}Ni_{0.6}Co_{0.4}O_2$ and $Na_{0.58}Ni_{0.6}Co_{0.4}O_2$, crystallize in the rhombohedral system. The packing types of these phases are $O3$ (space group $R\bar{3}m$) and $P3$ (space group $R3m$), respectively. As revealed in previous studies (5, 16), the intensity of the $(104)_{hex.}$ diffraction line is stronger than that of the $(015)_{hex.}$ line for the $O3$-type structure. The opposite is observed for the $P3$-type structure. The materials with intermediate composition ($O'3$- and $P'3$-type structures) crystallize in the monoclinic system.

In order to facilate comparison of the cell parameters, all materials were indexed in the monoclinic system. These monoclinic cell parameters are listed in Table 1. For the $O3$ and $P3$ phases, which have a rhombohedral symmetry, the hexagonal lattice parameters are related to the monoclinic cell parameters by the following relations:

$$a_{hex.} = a_{mon.}/\sqrt{3}; \quad b_{hex.} = b_{mon.}; \quad c_{hex.} = 3c_{mon.}\sin\beta.$$

As a result, one observes that the M–M intrasheet distances, given by both $a_{mon.}/\sqrt{3}$ and $b_{mon.}$, decrease and that the interslab distances ($c_{mon.}\sin\beta$) increase with decreasing sodium amount. These changes are in good agreement with those of most A_xMO_2 layered oxides and can be explained by the oxidation of the transition metal ions from M^{3+} to M^{4+} ($M = Ni_{0.6}Co_{0.4}$), and by the loss of lattice cohesion when sodium ions are removed from the interslab space. It is important to note that the $a_{mon.}/b_{mon.}$

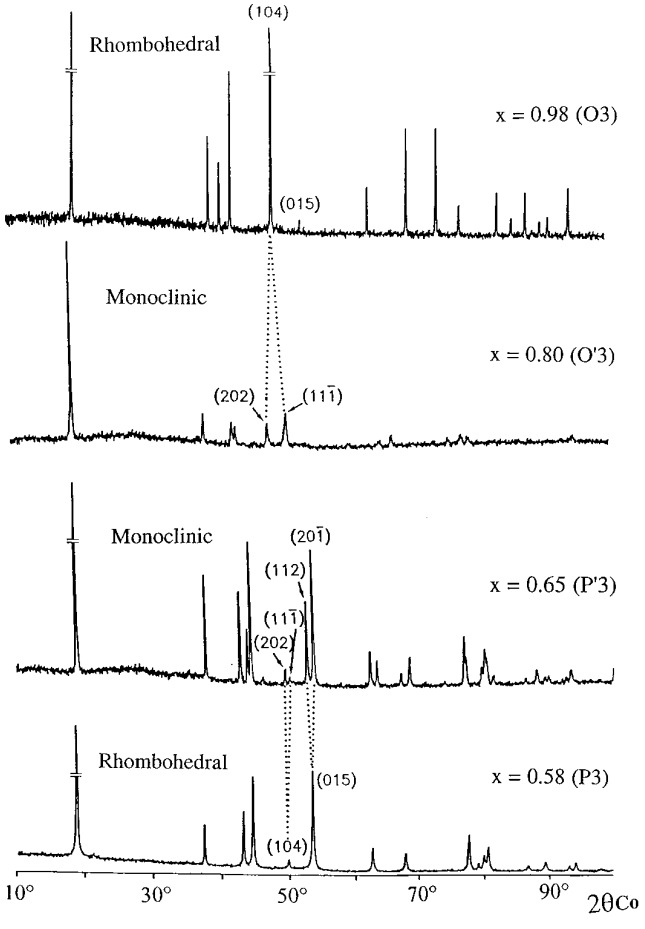

FIG. 2. X-ray diffraction patterns of the $Na_xNi_{0.6}Co_{0.4}O_2$ phases.

ratio, which reflects the magnitude of the lattice distortion, is more distant from the ideal $\sqrt{3}$ value (for which the lattice symmetry is rhombohedral) in the case of the $O'3$ solid solid ($a_{mon.}/b_{mon.} = 1.695$ for $x = 0.80$) compared to the $P'3$ one ($a_{mon.}/b_{mon.} = 1.73$ for $x = 0.65$). This structural difference explains the existence of a biphased domain (plateau at 2.25 V) between the O3 and $O'3$ solid solutions, whereas the $P'3 \rightarrow P3$ structural transformation occurs continuously without existence of a ($P'3 + P3$) biphased domain in the OCV composition curve. Nevertheless, one has to be prudent with the true symmetry of the $Na_{0.58}Ni_{0.6}Co_{0.4}O_2$ phase. From the X-ray powder pattern, a rhombohedral symmetry has been found; it may be that the monoclinic distortion is too small to be detected.

As mentioned for the Na_xCoO_2 system (17), the β value decreases during the $O3 \rightarrow O'3 \rightarrow P'3 \rightarrow P3$ transformation, indicating that the $O3 \rightarrow P3$ structural transition is due to the gliding motion of the $(Ni_{0.6}Co_{0.4}O_2)_n$ slabs with respect to each other. This evolution shows also that the $O'3$-type structure constitutes an intermediate stage of the $O3 \rightarrow P3$ transformation. A similar transformation has been observed during the structural study of the Na_xTiS_2 system (5), but the $O'3$-type phase has never been obtained in the case of chalcogenides (6, 7).

Physical Properties Study

The chemical deintercalation of the $NaNi_{0.6}Co_{0.4}O_2$ phase allows one to obtain a large quantity of product for the physical characterization. As intermediate $Na_xNi_{0.6}Co_{0.4}O_2$ ($0.58 < x < 1.0$) phases are difficult to prepare using the chemical method and as the electrochemical method does not give enough material, our physical study was limited to one composition of each structural type: $NaNi_{0.6}Co_{0.4}O_2$ ($O3$ phase), $Na_{0.58}Ni_{0.6}Co_{0.4}O_2$ ($P3$ phase), and $Na_{0.80}Ni_{0.6}Co_{0.4}O_2$ ($O'3$ phase). The last material has been obtained by the short circuit method from the stoichiometric mixture of the $NaNi_{0.6}Co_{0.4}O_2$ and $Na_{0.58}Ni_{0.6}Co_{0.4}O_2$ (18).

Figure 3 shows the temperature variation of the reciprocal magnetic molar susceptibility for the $Na_xNi_{0.6}Co_{0.4}O_2$ ($x = 1$, 0.80, 0.58) phases. The linearity of the $1/\chi_m$ vs T curve is typical of a Curie–Weiss paramagnetism, showing that the magnetic moments are localized. It should be noted that the slight deviation from linearity of the $1/\chi_m = f(T)$ curve for the two oxidized phases is due to the TIP contribution. The fit of the χ_m vs $1/T$ curve, according to the $\chi_m = C/(T - \theta p) + N\alpha$ equation, gives the following values: $C = 0.23$, $N\alpha = 200.10^{-6}$ emu-mol^{-1} (TIP contribution), $\theta p = 12$ K for the $Na_{0.80}Ni_{0.6}Co_{0.4}O_2$ phase and $C = 0.13$, $N\alpha = 100 \times 10^{-6}$ emu-mol^{-1}, $\theta p = 10$

TABLE 1
Monoclinic Cell Parameters of the $Na_xNi_{0.6}Co_{0.4}O_2$ Phases ($x = 1$, 0.98, 0.80, 0.65, 0.58); the Interslab Distance Is Equal to $c \sin \beta$

x_{Na}	$a \pm 0.005$ (Å)	$b \pm 0.003$ (Å)	$c \pm 0.01$ (Å)	$\beta \pm 0.01$ (°)	$c \sin \beta \pm 0.01$ (Å)	Symmetry
1	5.110	2.950	6.27	122.63	5.28	Rhombohedral
0.98	5.105	2.945	6.26	122.08	5.30	Rhombohedral
0.80	4.902	2.890	5.81	111.89	5.39	Monoclinic
0.65	4.890	2.826	5.70	106.44	5.47	Monoclinic
0.58	4.886	2.825	5.80	106.31	5.56	Rhombohedral

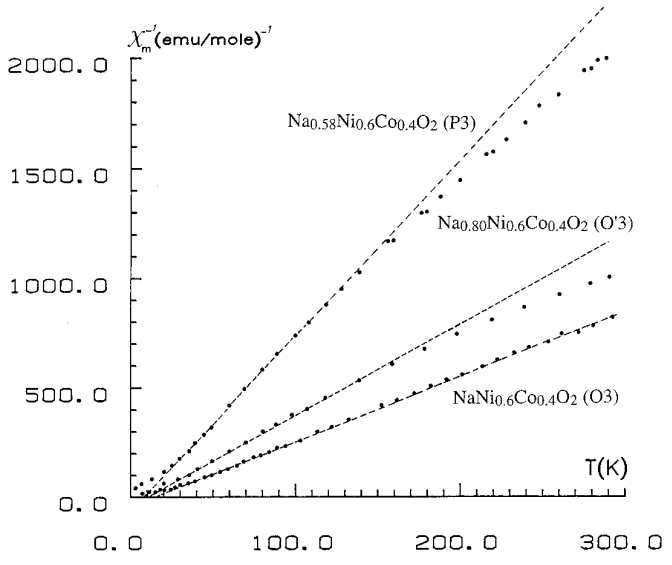

FIG. 3. Temperature variation of the reciprocal molar magnetic susceptibility of the $Na_xNi_{0.6}Co_{0.4}O_2$ ($x = 1$, 0.80, 0.58) phases.

K for the $Na_{0.58}Ni_{0.6}Co_{0.4}O_2$ phase. The magnetic results deduced from this study are listed in Table 2. The experimental Curie constant of the $NaNi_{0.6}Co_{0.4}O_2$ phase is in good agreement with a low-spin state configuration for Ni^{III} and Co^{III} ions. For the deintercalated phase, the theoretical Curie constants were calculated assuming either nickel or cobalt oxidation. They show that Ni^{III} ($t_2^6e^1$) ions are oxidized to Ni^{IV} preferentially to the Co^{III} ($t_2^6e^0$) ions. This result confirms those found for $Li_xNi_{1-y}Co_yO_2$ phases (9) and for the cobalt-substituted nickel oxyhydroxides (19). It shows that it is easier to remove the e^1 electron of the d^7 trivalent nickel ion (leading to the particularly stable d^6 LS configuration) than to remove one t_2 electron from the trivalent cobalt ion (t_2^6).

The positive θp values show that ferromagnetic interactions predominate, as in the unsubstituted $NaNiO_2$ material (8).

TABLE 2
Comparison of the Experimental and Calculated Curie Constants of the $Na_xNi_{0.6}Co_{0.4}O_2$ Phases

x in $Na_xNi_{0.6}Co_{0.4}O_2$	$C_{obs.}$	$C_{theo.}$		θp (K)
		C_1	C_2	
1.0	0.30	0.23	0.23	17
0.80	0.23	0.14	0.31	12
0.58	0.13	0.06	0.39	10

Note. C_1 corresponds to the trivalent nickel oxidation hypothesis ($Na_xNi^{III}_{x-0.4}Ni^{IV}_{1-x}Co^{III}_{0.4}O_2$) and C_2 corresponds to the trivalent cobalt oxidation hypothesis ($Na_xNi^{III}_{0.6}Co^{III}_{x-0.6}Co^{IV}_{1-x}O_2$).

The variation of the logarithm of the conductivity is plotted against reciprocal temperature in Fig. 4. For all samples, the shape the $\log \sigma = f(1000/T)$ curves shows clearly that the conduction phenomenon is thermally actived. This result confirms that the $Na_xNi_{0.6}Co_{0.4}O_2$ ($x = 1$, 0.80, 0.58) phases have localized d electrons. Nevertheless, the conductivity increases with decreasing sodium amount. As previously demonstrated, the electrical behavior of the $NaNi_{0.6}Co_{0.4}O_2$ phase could be well explained by the energy diagram proposed for the $NaNiO_2$ nickelate (20). The activation energy of this substituted phase would correspond to the difference in energy between the top of the oxygen level and the Ni^{3+}/Ni^{2+} unoccupied level. For the $Na_xNi_{0.6}Co_{0.4}O_2$ ($x = 0.80$, 0.58) oxidized phases, the shape of the $\log \sigma$–$1000/T$ curve is typical of a small polaron conduction mechanism generally observed in a mixed valence system. The presence of Ni^{III} and Ni^{IV} ions in the $Na_xNi_{0.6}Co_{0.4}O_2$ ($x = 0.80$, 0.58) materials, which allows an easy electronic transfer via hopping, and the more covalent character of the $(Ni_{0.6}Co_{0.4}O_2)_n$ sheets may explain the increase in the electronic conductivity with decreasing sodium amount. The electronic localization in the $Na_xNi_{0.6}Co_{0.4}O_2$ ($x = 0.80$, 0.58) phases confirms the absence of an oxidation of the trivalent cobalt ions. In fact, the presence of tetravalent cobalt ions allows electronic delocalization as already observed in the $Li_xNi_{0.1}Co_{0.9}O_2$ system (21).

Diffusion Kinetics

In an attempt to reveal the dependence of the diffusion kinetics on the sodium environment in the $Na_xNi_{0.6}Co_{0.4}O_2$

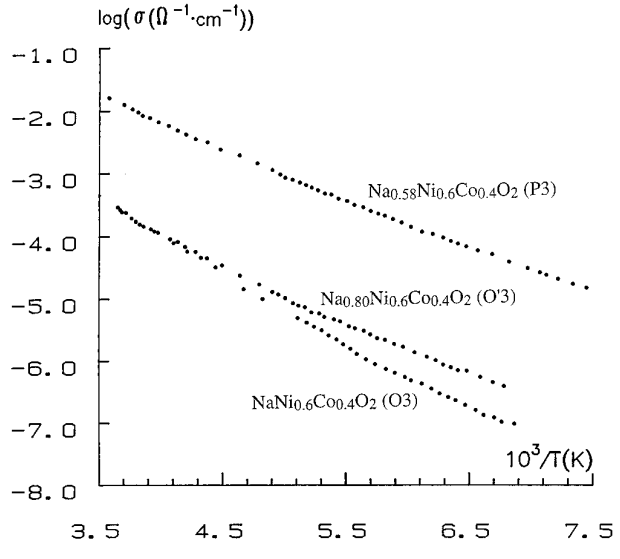

FIG. 4. Variation of the logarithm of the conductivity vs reciprocal temperature of the $Na_xNi_{0.6}Co_{0.4}O_2$ ($x = 1$, 0.80, 0.58) phases.

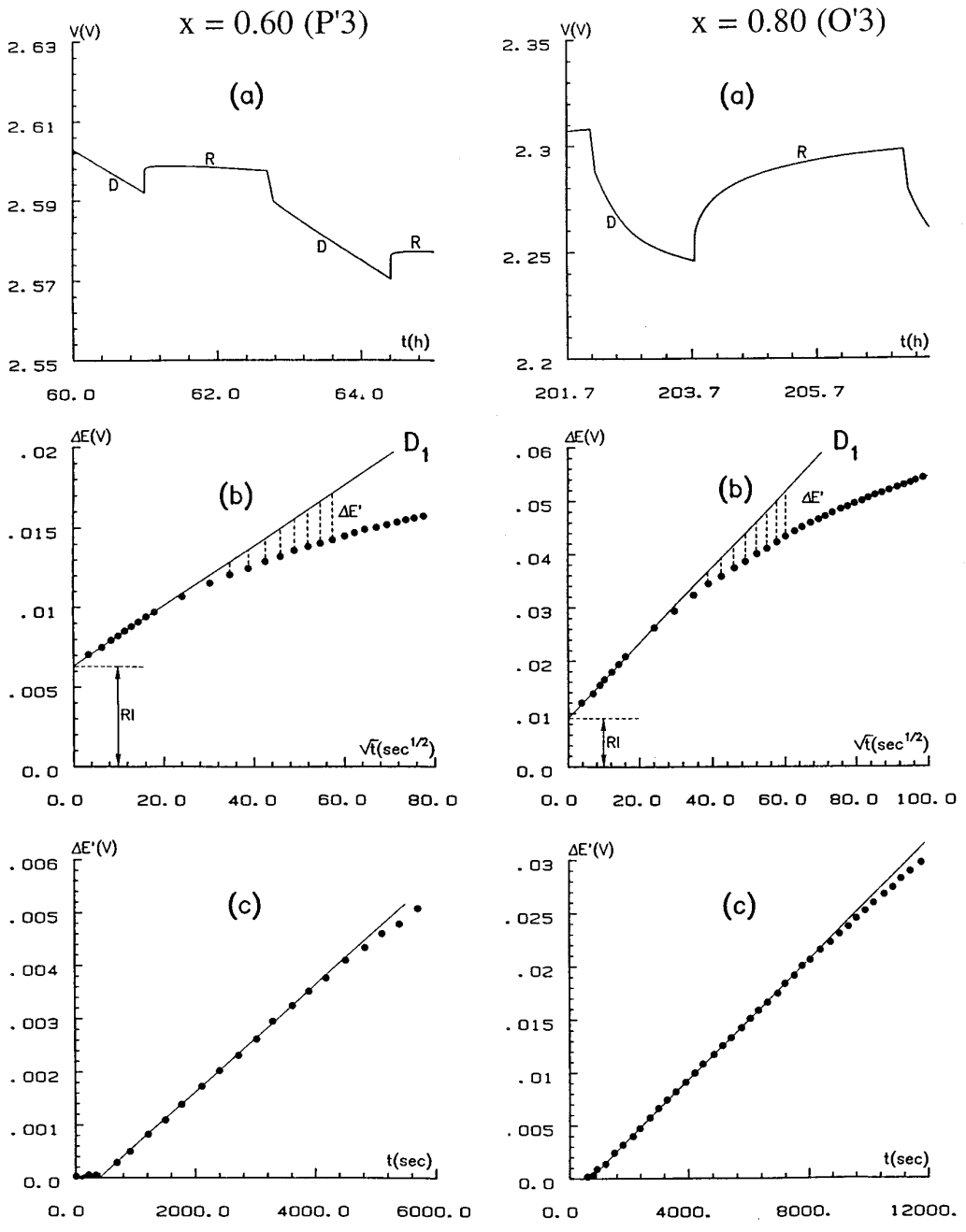

FIG. 5. Variation of ΔE (b) and $\Delta E'$ (c) vs time, extracted from the discharge curves reported in (a), for two $Na_xNi_{0.6}Co_{0.4}O_2$ compositions ($x = 0.60, 0.80$). (As a result of the very different diffusion coefficients, the scales of the x and y axes are different for both compositions.)

phases, chemical diffusion coefficients of Na^+ ions were determined using Honder's method (22), in the solid solution domains. This method utilizes the relaxation periods after long discharge times of the $Na\|Na_xNi_{0.6}Co_{0.4}O_2$ cell. In these solid solution domains, the variation of potential upon relaxation is essentially due to the homogenization of the sodium concentration within the grains. It can be expressed according to Fick's second law:

$$\Delta E = \left(\frac{Ak_t}{S}\right)\left[\left(\frac{4t}{\pi D}\right)^{1/2} - \frac{t}{\delta}\right],$$

where

A is a constant;
k_t is the Darken factor defined by $k_t = dlna/dlnc$;

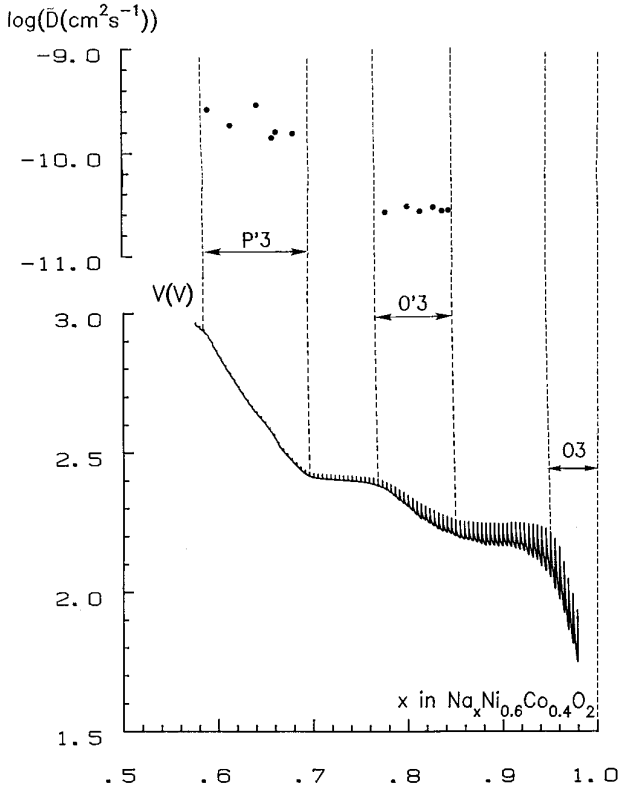

FIG. 6. Variation of the chemical diffusion coefficient vs the amount of sodium in the $Na_xNi_{0.6}Co_{0.4}O_2$ phases, compared with the OCV discharge curve.

S is the contact area of the electrode with the electrolyte;
D is the chemical diffusion coefficient of the intercalated species; and
δ is the electrode depth (the electrode being considered as a homogenous block in which semi-infinite diffusion takes place).

For the small values of time (for which t/δ is negligible compared to the $(4t/\pi D)^{1/2}$ term), the $\Delta E = f(\sqrt{t})$ curve is linear (D_1) with a $p_1 = (2Ak_t)/S(\pi D)^{1/2}$ slope. It should be noted that the extrapolation of the D_1 straight line for $t = 0$ yields the true ohmic drop of the cell which is due to the electronic resistance of the positive electrode material and the ionic resistance of the electrolyte.

The fact that the IR drop is measured at the circuit opening, i.e., in a nonhomogeneous electrode, leads to questionable interpretations. However, in the present case, a clear variation is seen. Whereas the IR drop is approximately constant within each of the three solid solution domains, it increases clearly from $P'3$ (6 mV) to $O'3$ (10 mV) and again to $O3$ (40 mV), which correlates well with the conducitivity data shown in Fig. 4.

Obviously, p_1 contains the D coefficient, but also k_t and S. Nevertheless, the difference ($\Delta E'$) between ΔE and D_1 (Fig. 5c) can be described by $\Delta E' = (Ak_t/S\delta)t$. Thus, the $\Delta E' = f(t)$ curve is a straight line, for larger values of time, with a slope $p_2 = (Ak_t/S\delta)$. The chemical diffusion coefficient can then easily be deduced from the ratio of the two slopes: $D = (2p_2\delta)^2/\pi p_1$. Figure 5 shows the curves representing the various steps, described above, necessary for the chemical diffusion coefficient calculations of two selected phases: $Na_{0.60}Ni_{0.6}Co_{0.4}O_2$ and $Na_{0.80}Ni_{0.6}Co_{0.4}O_2$ belonging to the $P'3$ and $O'3$ solid solution domains, respectively.

Note that, in the present case of an electrode consisting of grains wetted by the liquid electrolyte, the electrode depth is best represented as the grain size. However, since the latter is not precisely known (δ has been measured as 5 μm from SEM pictures), the values of the sodium chemical diffusion coefficients cannot be considered the absolute values. Nevertheless, we can reasonably discuss and interpret their changes with sodium amount in $Na_xNi_{0.6}Co_{0.4}O_2$ phases, since the results were carried out with the same electochemical cell. It should be note that the application of Honder's method requires an important condition: the discharge duration must be larger than $(0.25\delta^2/D)$. As this condition can virtually not be reached in the narrow $O3$ solid solution, we have not reported the D values calculated in this composition domain in Fig. 6. However, one can conclude from such behavior that D is particularly low in this domain.

Figure 6 reports the variation of D coefficients vs x for some $Na_xNi_{0.6}Co_{0.4}O_2$ compositions. In the $P'3$ and $O'3$ solid solution domains, the diffusion coefficient remains almost constant. Yet it is clear that the sodium chemical diffusion coefficient is higher in the case of the $P'3$ solid solution. A similar evolution was shown by Maâzaz (23) and Trichet and Rowel (24) in their studies on the relation between structural aspect and ionic conductivity of alkali metal in layered oxides and the $Na_xIn_xZr_xS_2$ system, respectively.

Our result can be explained if we consider the diffusion pathway in the two cases. In the $O'3$-type structure, the diffusion of sodium from one octahedron to another requires a transit via one tetrahedron, i.e., via two triangular faces. In contrast, in the $P'3$-type structure, the transit occurs through one rectangular face. It is evident that in the first case ($O'3$-type solid solution), the steric repulsions are stronger than in the second case. Hence, the sodium chemical diffusion coefficient is lower in the $O'3$ solid solution domain.

REFERENCES

1. M. G. S. R. Thomas, W. I. F. David, J. B. Goodenough, and P. Groves, *Mater. Res. Bull.* **20,** 1137 (1985).
2. K. M. Abraham, *Solid State Ionics* **7,** 199 (1982).
3. M. S. Whittingham, *J. Electrochem. Soc.* **123,** 315 (1976).

4. C. Delmas, ''Chemical Physics of Intercalation'' (A. P. Legrand and S. Flandrois, Eds.), NATO ASI Series, Vol. 172, p. 209. Plenum, New York, 1987.
5. J. Rouxel, M. Danot, and J. Bichon, *Bull. Soc. Chim. Fr.,* 3930 (1971).
6. D. A. Winn, J. M. Shemilt, and B. C. H. Steele, *Mater. Res. Bull.* **11,** 559 (1976).
7. A. S. Nagelberg and W. L. Worrell, *J. Solid State Chem.* **29,** 345 (1979).
8. L. D. Dyer, B. S. Borie, J. R. Smith, and G. P. Smith, *J. Am. Chem. Soc.* **76,** 1499 (1954).
9. I. Saadoune, Thesis, University of Bordeaux I, 1992.
10. S. Miyazaki, S. Kikkawa, and M. Koizumi, *Synth. Met.* **6,** 211 (1983).
11. C. Delmas, Y. Borthomieu, C. Faure, A. Delahaye, and M. Figlarz, *Solid State Ionics* **32/33,** 104 (1989).
12. C. Delmas, J. J. Braconnier, C. Fouassier, and P. Hagenmuller, *Solid State Ionics* **3/4,** 165 (1981).
13. G. Millazo, ''Electrochemistry, Theoretical and Practical Applications.'' Elsevier, Amsterdam, 1962.
14. C. Delmas, I. Saadoune, and A. Rougier, *J. Power Source* **43/44,** 595 (1993).
15. J. J. Braconnier, C. Delmas, C. Fouassier, and P. Hagenmuller, *Mater. Res. Bull.* **15,** 1797 (1980).
16. C. Fouassier, G. Matejka, J. M. Reau, and P. Hagenmuller, *J. Solid State Chem.* **60,** 532 (1973).
17. L. W. Shackelette, T. R. Jow, and L. Townsend, *J. Electrochem. Soc.* **135,** 2669 (1988).
18. A. Nadiri, Thesis, University of Bordeaux I, 1986.
19. Y. Borthomieu, Thesis, University of Bordeaux I, 1990.
20. C. Delmas, I. Saadoune, and P. Dordor, *Mol. Cryst. Liq. Cryst.* **244,** 337 (1994).
21. C. Delmas and I. Saadoune, *Solid State Ionics* **53,** 370 (1992).
22. A. Honders, J. M. Der Kinderen, A. H. Van Heeren, J. H. W. De Wit, and G. H. J. Broers, *Solid State Ionics* **15,** 265 (1985).
23. A. Maâzaz, Thesis, University of Bordeaux I, 1982.
24. L. Tichet and J. Rouxel, *Mater. Res. Bull.* **12,** 345 (1977).